PHILOSOPHICAL TRANSACTIONS A

royalsocietypublishing.org/journal/rsta

Research

Cite this article: Thiébaut M, Filipot J-F, Maisondieu C, Damblans G, Jochum C, Kilcher LF, Guillou S. 2020 Characterization of the vertical evolution of the three-dimensional turbulence for fatigue design of tidal turbines. *Phil. Trans. R. Soc. A* **378**: 20190495. http://dx.doi.org/10.1098/rsta.2019.0495

Accepted: 23 April 2020

One contribution of 14 to a theme issue 'New insights on tidal dynamics and tidal energy harvesting in the Alderney Race'.

Subject Areas:
geophysics, fluid mechanics, oceanography

Keywords:
turbulence, Reynolds stresses, tidal-steam energy convertor, coupled acoustic Doppler current profilers, Alderney Race

Author for correspondence:
Maxime Thiébaut
e-mail: Maxime.Thiebaut@ite-fem.org

Electronic supplementary material is available online at https://doi.org/10.6084/m9.figshare.c.5013530.

THE ROYAL SOCIETY PUBLISHING

Characterization of the vertical evolution of the three-dimensional turbulence for fatigue design of tidal turbines

Maxime Thiébaut[1], Jean-François Filipot[1], Christophe Maisondieu[2], Guillaume Damblans[1], Christian Jochum[3], Levi F. Kilcher[4] and Sylvain Guillou[5]

[1]France Énergies Marines, Technopôle Brest-Iroise, 525 Avenue Alexis de Rochon, 29280 Plouzané, France
[2]IFREMER, ZI Pointe du diable, 29280 Plouzané, France
[3]ENSTA Bretagne, CNRS UMR 6027, IRDL, 2 rue Francois Verny, 29806 Brest, France
[4]National Renewable Energy Laboratory, Golden, CO, USA
[5]Normandie Univ, UNICAEN, LUSAC, EA4253, site universitaire de Cherbourg, rue Louis Aragon, BP 78, 50130 Cherbourg-Octeville, France

MT, 0000-0001-9316-6437; J-FF, 0000-0003-0875-8791

A system of two coupled four-beam acoustic Doppler current profilers was used to collect turbulence measurements over a 36-h period at a highly energetic tidal energy site in Alderney Race. This system enables the evaluation of the six components of the Reynolds stress tensor throughout a large proportion of the water column. The present study provides mean vertical profiles of the velocity, the turbulence intensity and the integral lengthscale along the streamwise, spanwise and vertical direction of the tidal current. Based on our results and considering a tidal-stream energy convertor (TEC) aligned with the current main direction, the main elements of turbulence prone to affect the structure (material fatigue) and to alter power generation would likely be: (i) the streamwise turbulence intensity (I_x), (ii) the shear stress, $\overline{v'w'}$, (iii) the normal stress, $\overline{u'^2}$ and (iv) the vertical integral lengthscale (L_z). The

streamwise turbulence intensity, (I_x), was found to be higher than that estimated at other tidal energy sites across the world for similar height above bottom. Along the vertical direction, the length (L_z) of the large-scale turbulence eddies was found to be equivalent to the rotor diameter of the TEC Sabella D10. It is considered that the turbulence metrics presented in this paper will be valuable for TECs designers, helping them optimize their designs as well as improve loading prediction through the lifetime of the machines.

This article is part of the theme issue 'New insights on tidal dynamics and tidal energy harvesting in the Alderney Race'.

1. Introduction

Nowadays, multiple options exist for lowering greenhouse gas emissions from the energy system while still satisfying the global demand for energy services. Nuclear power is one of them, but there is concern among the public in many countries about its safety, and the issue of decommissioning and disposal of nuclear waste concerns nuclear engineers as well as the public. The exploitation of renewable energy resources appears as a valuable alternative. It has great potential to mitigate climate change and can provide wider benefits such a contribution to social and economic development, a secure energy supply and reducing negative impacts on the environment and health.

Deployment of renewable energy technologies has increased rapidly in recent years. Among them, the development of ocean energy conversion systems has witnessed significant growth. Tidal current energy conversion has been noted as one of the viable technologies for its inherent predictability and reliability. However, the development of the tidal energy industry still lags behind wind or solar energy industry. The delayed development of tidal energy is mainly due to harsher environmental conditions encountered by tidal-stream energy converters (TECs) such as salt-induced corrosion, extreme turbulence or strong currents, affecting deployment and maintenance operations [1]. These environmental constraints affect the physical integrity of TECs and raise many uncertainties with regard to the cost-effectiveness of any project of tidal energy conversion.

Failures of early generation TECs have been cited to be a consequence of a poor understanding of the magnitudes and the spectral characteristics of the turbulence-induced hydrodynamic loads [2,3]. Thus, a better understanding of the nature of turbulence in tidal channels is a key goal in the successful installation, operation and maintenance strategies of TECs. In order to gain confidence in the prediction of the hydrodynamics loading and prevent unexpected failures, measurements of ambient turbulence (i.e. natural turbulence before the installation of TEC) is critical. An accurate characterization of both the mean turbulence quantities and their variability is needed to reduce the risk associated with uncertainty in the flow conditions. For such study, four or five beam acoustic Doppler current profilers (ADCPs) are among the most widely-used instruments (e.g. [4–10]). ADCPs use the Doppler shift in the echoes of pings along directed acoustic diverging-beams to measure flow velocities.

The popularity of ADCPs has considerably increased since Lohrmann *et al.* [11] introduced the so-called variance method. With this technique, Reynolds stress profiles are estimated from along-beam velocity measurements, using the difference between the velocity variances along opposing beams, often with explicit removal of the variance induced by the Doppler noise. However, the non-homogeneous nature of the flow, coupled with the horizontal spreading of the ADCP beams, imposes a restriction on the turbulence lengthscales that can be studied accurately. At a given depth, the beam spread or beam separation may be interpreted as the minimum lengthscale of turbulence that is measured accurately by an ADCP. Assuming a bottom-mounted ADCP, the beam spread increases with increasing height above bottom and can exceed the rotor diameter of a TEC (i.e. up to 20 m). The estimation of turbulence metrics requires that the second-order moments of fluctuating velocities be horizontally homogeneous so that the statistics of the turbulence are the same for each beam [12]. Such an assumption is required when using a single four-beam ADCP since it provides only two components (out of six) of the Reynolds stress tensor.

Recently, Thiébaut *et al.* [13] deployed two four-beam ADCPs operating in master-slave configuration at a tidal energy site in Alderney Race. With the beam combination of the two coupled sensors, eight beams are available allowing for the resolution of the six components of the Reynolds stress tensor as well as an improved estimation of the turbulent kinetic energy (TKE) production rate $\mathcal{P}$. Evaluation of the latter, together with the TKE dissipation rate ε enabled the determination of an approximate TKE budget. The depth-averaged ratio $\varepsilon/\mathcal{P}$ averaged over whole flood and ebb tide were found to be higher than 2 for both tidal phases, indicating that TKE dissipation exceeds TKE production at the measurement site.

The present study is an extension of the work initiated by Thiébaut *et al.* [13,14]. The following metrics are quantified: (i) the velocity, (ii) the turbulence intensity, (iii) the integral lengthscale and (iv) the six components of the Reynolds stresses. All metrics are evaluated in three dimension (3D), i.e. along the streamwise, spanwise and vertical velocity. There is broad agreement that these turbulence metrics contribute significantly to turbulence-induced hydrodynamics loads on TECs. The aim of this study is to provide modellers and TEC designers with mean profiles of the turbulence metrics throughout the water column allowing them to build a dedicated methodology for fatigue life prediction of moving components at one of the most promising tidal energy sites across the world [15–17]. This work provides relevant insights representing the necessary basis to define a 3D scatter diagram of couples (stress, frequency) with the associated occurrence in order to perform standard modal fatigue computations.

2. Data analysis and methods

(a) Experimental settings

Two upward-looking RDI Workhorse 600 kHz four-beam ADCPs were deployed on the seafloor (mean and maximum water depth of 31 m and 35 m, respectively) approximately 4 km offshore, west of the port of Goury, in the eastern part of Alderney Race, France (figure 1) [13,14]. The instruments were mounted on a specifically designed frame having the following features: 3.3 m long, 2.5 m wide and 2 100 kg weight (figure 1). The ADCPs collected data over a 38-day period, from 27 September to 3 November 2017. The instruments were coupled in a master-slave set-up and were set to record alternately the along-beam velocities at the pinging rate of 2 Hz. This measurement scheme was chosen in order to avoid any interference between the beams of the two sensors. Velocities were recorded with 1.3 m vertical resolution (bin size), starting 2.2 m from the seafloor (the first bin). The average standard deviation of the attitude parameters (heading θ_h, pitch θ_p and roll θ_r) of the master ADCP were found to be lower than 0.3°, indicating that the frame remained stable throughout the deployment.

A Cartesian coordinates system ($\mathcal{O}$, $\boldsymbol{e_x}$, $\boldsymbol{e_y}$, $\boldsymbol{e_z}$) was defined relative to the master ADCP, with the origin $\mathcal{O}$ located at the centre of the four transducers (figure 1). The average heading of the master ADCP was such that the opposite beams 1 and 2 were oriented in the streamwise direction, defining the $\boldsymbol{e_x}$-axis, whereas beams 3 and 4 pointed in the spanwise direction, defining the $\boldsymbol{e_y}$-axis. The slave ADCP was rotated relative to the master and they were located 0.5 m apart horizontally, following the set-up proposed by Vermeulen *et al.* [18]. The slave ADCP was rotated 45 degrees around the $\boldsymbol{e_z}$-axis, and 20 degrees around the $\boldsymbol{e_x}$-axis, resulting in a tilted ADCP with one beam pointed vertically upward (figure 1). This orientation is the best compromise between reasonable errors in the Reynolds stresses estimates and the surface reflection which generate unusable velocity measurements [18].

(b) Analysis techniques

The present study focuses on turbulence characterization along the streamwise (u), spanwise (v) and vertical (w) direction. Velocities were derived from measurements of the master ADCP by applying the product of the along-beam velocities with a transformation matrix given in [19].

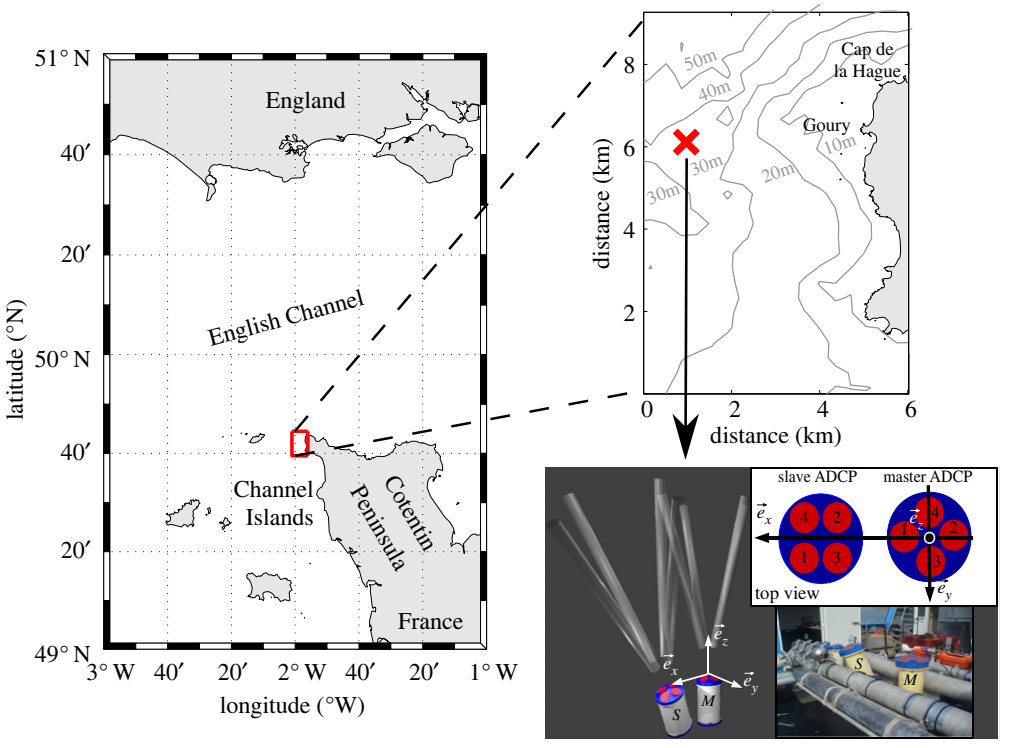

Figure 1. Left-hand side panel: map of the central part of the English Channel. Top right-hand side panel: the eastern part of Alderney Race with bathymetry (m) given in grey. Red cross denotes the location of the master and slave bottom-mounted ADCPs deployment site. Bottom right-hand side panel: three-dimensional view of the experimental set-up (left-hand side) with the top view enclosed on the right-hand side. The letters 'S' and 'M' stand for slave and master ADCP, respectively. The Cartesian coordinates system is defined relative to the master with the origin located at the centre of the four transducers (red circles). The beam numbering is shown in the $\boldsymbol{e_x} - \boldsymbol{e_y}$ plane in the upper right-hand side panel. A photograph of the experimental set-up before the deployment is also enclosed. (Online version in colour.)

In order to avoid any wave contamination in turbulence measurements, a period where wave orbital motions are negligible was selected for the analysis. Such a period was identified between 1 November 2017—01.45 UTC and 2 November 2017—13.45 UTC. During this 36-h long period the mean significant height H_s and mean peak period T_p were found to be 0.6 m and 6 s, respectively.

For such a peak period, the increased variance associated with the wave motion does not penetrate to depths greater than 10 m [13]. Thus, the 10-m thick uppermost surface layer was not considered in this study. Only the water layer ranging between 3.5 metre above bottom (m.a.b) and 20.4 m.a.b was considered in this analysis. Hereafter, the term 'depth-averaged' refers to the averaging within this water layer which includes the operating water layer of a TEC such as the Sabella D10 (http://www.sabella-d10.bzh). At the time of writing, this machine is deployed in the centre of the Fromveur Strait, France, where the mean and maximum flow speed are of similar order of magnitude as that recorded in Alderney Race [20].

The 36-h long period was divided into 226 subsets of 10-min each. 'Slack conditions', where the velocity magnitude did not exceed 0.8 m s^{-1}, were excluded from the analysis since they are not operationally relevant for TECs (i.e. below 'cut-in' speed) [5,21,22]. As a result, 16% of the 10-min subsets were rejected. Hereafter, an overbar is used to represent a temporal average over each subset. The 10-min duration is of sufficient length to provide a good sample of the largest turbulent eddies, but not so long that the turbulent processes cannot be regarded as quasi-stationary.

(c) Turbulence intensity

Turbulence intensity is a common metric used throughout wind and tidal industry as well as other engineering fields in order to quantify turbulence. It is given by

$$I_i = \frac{\sqrt{\sigma_i^2 - \sigma_{N_i}^2}}{U}, \tag{2.1}$$

where $U = \sqrt{u^2 + v^2 + w^2}$ is the mean flow speed (σ_i^2) is the variance associated with the streamwise, spanwise and vertical velocities and ($\sigma_{N_i}^2$) is the variance induced by Doppler noise. ($\sigma_{N_i}^2$) was estimated from the energy-spectra of the velocities [13].

The uncertainty, (ϵ_{I_i}), when calculating the mean turbulence intensity, was resolved through the computation of the standard error of the mean. The latter is the ratio of the standard deviation to the square root of the sample size, i.e. the number of subsets in our study. The standard error of the mean is a way to validate the accuracy of a sample by analysing deviation within the means. It describes how precise the mean of the sample is versus the true mean of the population. The smaller the spread, the more accurate the dataset.

(d) Integral lengthscale

The integral lengthscale, (L_i), was estimated from the calculation of the integral timescale, (Λ_i). The latter is a measure of the duration for which the largest eddies remain correlated. For each 10-min interval, (Λ_i) is computed from a temporal autocorrelation function, $R_{ii}(\tau)$, integrated with respect to time between the limits, $\tau = 0$, and the first instance of $R_{ii} = 1/e$, such that [23]

$$\Lambda_i = \int_{\tau=0}^{\tau[R_{ii}(\tau)=1/e]} R_{ii}(\tau)\,\mathrm{d}\tau, \tag{2.2}$$

where $e = \exp(1)$. Note that an alternative method is to integrate the autocorrelation function up to the first zero-crossing (e.g. [24]). However, in our study, only 9%, 47% and 31% of the autocorrelation functions associated with the streamwise, spanwise and vertical velocity, respectively, met the condition $R_{ii}(\tau) = 0$. By comparison, the condition $R_{ii}(\tau) = 1/e$ was, respectively, met by 85%, 99% and 97% of the autocorrelation functions. This result justifies our choice to set the upper limit of the integral to the first instance where $R_{ii}(\tau) = 1/e$ instead of $R_{ii}(\tau) = 0$. The integral lengthscales derived from the autocorrelation functions which did not meet the condition $R_{ii}(\tau) = 1/e$ were rejected.

In the streamwise direction, the temporal autocorrelation function is expressed as:

$$R_{uu}(\tau) = \frac{R[u'(t), u'(t+\tau)]}{\sigma_u^2}, \tag{2.3}$$

where the prime denotes a fluctuation from the mean. The temporal autocorrelation function along the spanwise and vertical, i.e. R_{vv} and R_{ww}, respectively, are obtained by replacing (u) by (v) and (w) in the above equation.

The integral lengthscale, (L_i), is estimated by invoking Taylor's frozen turbulence hypothesis

$$L_i = \Lambda_i U. \tag{2.4}$$

The uncertainty, (ϵ_{L_i}), was resolved through the calculation of the standard error of the mean.

(e) Variance method for coupled acoustic Doppler current profilers

The coupled ADCPs method developed by Vermeulen *et al.* [18] combines, (i), the traditional transformation method, where two opposite beams of the ADCP are used to transform velocities in beam coordinates to velocities in Cartesian coordinates system, with (ii), the rotation of the

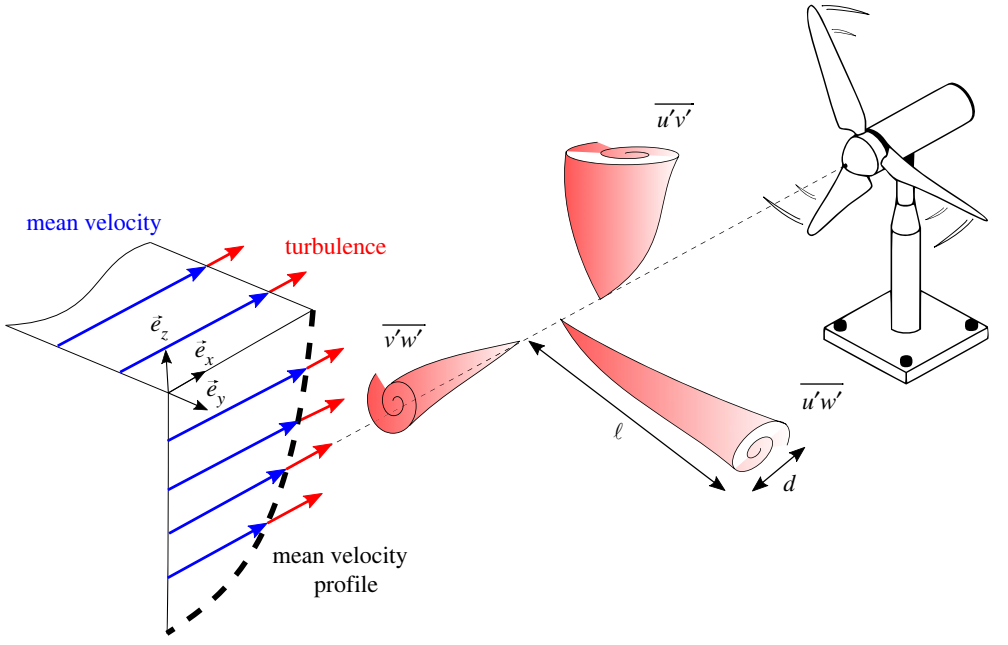

Figure 2. Schematic of turbulent inflow to a tidal-stream energy converter. The mean-flow profile is represented in blue, and turbulent eddies of different characteristic sizes (d), lengths (ℓ) and orientations are indicated in red. (Online version in colour.)

slave relative to the master ADCP. The velocities in beam coordinates equates to the velocities (u, v, w) in Cartesian coordinates as

$$\boldsymbol{B} = T\mathbf{u}, \tag{2.5}$$

where $\boldsymbol{B}$ is an eight-component vector containing all the radial velocity components from the two coupled ADCPs, $\mathbf{u}$ is the velocity vector in the Cartesian coordinates system ($\mathbf{u} = u\boldsymbol{e_x} + v\boldsymbol{e_y} + w\boldsymbol{e_z}$) and (T) is the transformation matrix given in the appendix. The velocities in the Cartesian coordinates system are obtained by inverting the transformation matrix (T). Note that (T) depends on the instruments used and the relative rotation of the slave ADCP.

The Reynolds stresses indicate the orientation of the eddies in the flow. Several studies have found evidence that Reynolds stresses are correlated with increased wind turbine fatigue loads (e.g. [25,26]). A significant contribution of Reynolds stresses to TEC fatigue loads is thus expected. Eddies of different orientations may impart forces on distinct components of a TEC. Considering a horizontal axis TEC, an eddy aligned with the rotor ($\overline{v'w'}$ in figure 2) might impart larger torque on the rotor shaft than eddies of other orientations, whereas $\overline{u'v'}$ and $\overline{u'w'}$ might induce bending and torque on the blades.

In order to obtain the components of the Reynolds stress tensor from the velocity variances in beam coordinates, a new eight by six matrix, (Q), is computed. (Q) results from the product of the terms in (T) such that

$$Q = T_{p,q}T_{p,m}, \tag{2.6}$$

where $p = [1;8]$ and $q, m = [1;3]$. (Q) allows relating the vector $\boldsymbol{v_B}$, containing the velocity variances in beam coordinates to the vector $\boldsymbol{r}$ containing the six terms of the Reynolds stress tensor as

$$\boldsymbol{v_B} = Q\boldsymbol{r}. \tag{2.7}$$

The six-element vector $\boldsymbol{r}$ can be rearranged to form the Reynolds stress tensor according to

$$\mathbf{R} = \begin{pmatrix} r_1 & r_4 & r_5 \\ r_4 & r_2 & r_6 \\ r_5 & r_6 & r_3 \end{pmatrix} = \begin{pmatrix} \overline{u'^2} & \overline{u'v'} & \overline{u'w'} \\ \overline{u'v'} & \overline{v'^2} & \overline{v'w'} \\ \overline{u'w'} & \overline{v'w'} & \overline{w'^2} \end{pmatrix}. \tag{2.8}$$

The uncertainty, $(\epsilon_{R_{p,n}})$, in the Reynolds stress estimates is given by Vermeulen *et al*. [18]

$$\epsilon^2_{R_{p,n}} = \frac{2}{M} \sum_{p=1}^{8} \left(Q^+_{p,n} v_{B_p} \right)^2 \quad (n = 1, \ldots, 6), \tag{2.9}$$

where $Q^+ = (Q^{\mathrm{T}}Q)^{-1}\, Q^{\mathrm{T}}$ with Q^{T} being the transpose of (Q) and (v_{B_p}) is the magnitude of the velocity vector $\boldsymbol{v_B}$, recorded along the pth beam. (M) is the number of samples contained within each 10-min subset, i.e. $M = 1200$ measurement points.

(f) Velocity spectra

Energy-spectra of the velocity (hereafter referred to as 'spectra') allow us to determine the distribution of turbulent energy as a function of frequency, i.e. spectra quantify the amount of energy in the flow at a range of timescales. Using Taylor's assumption of frozen turbulence, timescales can be converted into lengthscales. As a result, spectra are now quantifying the distribution of turbulent energy at different lengthscales, i.e. the energy (rotation speed) of eddies as a function of their characteristic size (d in figure 2). Note that (d) is not quantified in this study.

In the present study, spectra of the streamwise, spanwise and vertical velocity were estimated from fast Fourier transforms of the turbulent velocity. Hamming window intervals of 120 points with 50% overlap were used giving 18 equivalent degrees of freedom for each estimate.

3. Results

(a) Velocity profiles

Vertical profiles of the streamwise (u), spanwise (v) and vertical (w) velocity were computed (figure 3*a*). The streamwise velocity increases with increasing height above bottom whereas the spanwise and vertical velocity remains nearly-constant throughout the water column. The depth-averaged value of the streamwise velocity was found to be $2.3\,\mathrm{m\,s^{-1}}$ whereas that of the spanwise and the vertical velocity were found to be 8 and 13 times lower, respectively ($0.3\,\mathrm{m\,s^{-1}}$ and $0.17\,\mathrm{m\,s^{-1}}$).

Figure 4*a* shows time series of the sea surface height (SSH) and the streamwise velocity recorded at height matching the hub of the Sabella D10 ($z = 12$ m.a.b). Tidal variations of SSH and currents are predominantly semi-diurnal and globally symmetric. Peak flood and ebb tidal velocities occur at high and low water levels, respectively, with slack water at mid-tide, the tidal current dynamics is thus referred to as progressive wave system.

(b) Turbulence intensity

The turbulence intensities were corrected from Doppler noise resulting in a mean reduction of the streamwise (I_x), spanwise (I_y) and vertical (I_z) turbulence intensity by 10%, 15% and 6%, respectively. The Doppler noise was found to be increasing with increasing flow speed and to be independent of the height above bottom (results not shown). More results regarding the quantification of the Doppler noise associated with this dataset can be found in [14].

Figure 3*b* shows the variation of the turbulence intensity (I_i) throughout the water column. The three components of the turbulence intensity decrease with increasing height above bottom. Higher turbulence intensities were found near the bottom, at depth lower than 5 m.a.b. There, the lowest values of the velocities were exhibited (figure 3*a*). The streamwise turbulence intensity

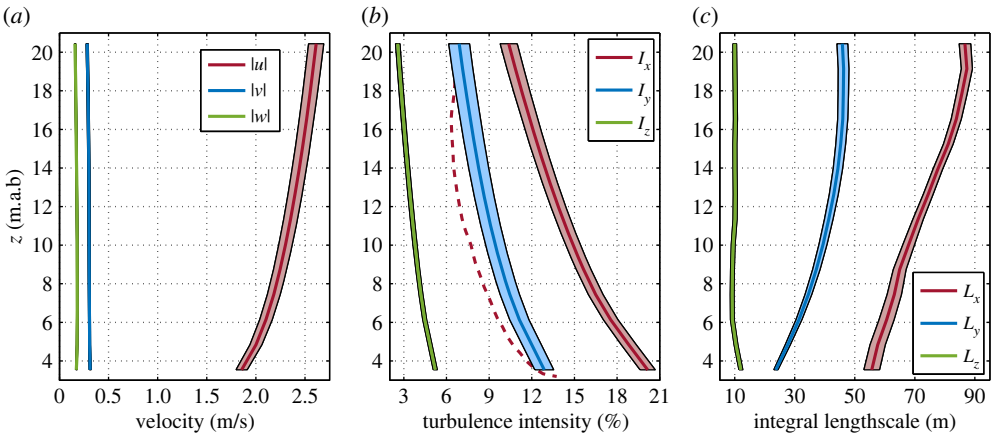

Figure 3. Mean vertical profiles (thick lines) of the velocity (*a*), turbulence intensity (*b*), and integral lengthscale (*c*), estimated along the streamwise, spanwise and vertical direction. Shading colours are used to identify the uncertainty (ϵ) associated with each metrics. Red dashed line in (*b*) is the mean profile of the streamwise turbulence intensity (I_x) derived from ADCP measurements performed by Thomson *et al.* [5] in Puget Sound, US. Numeric values used to build the profiles are provided alongside the present paper. (Online version in colour.)

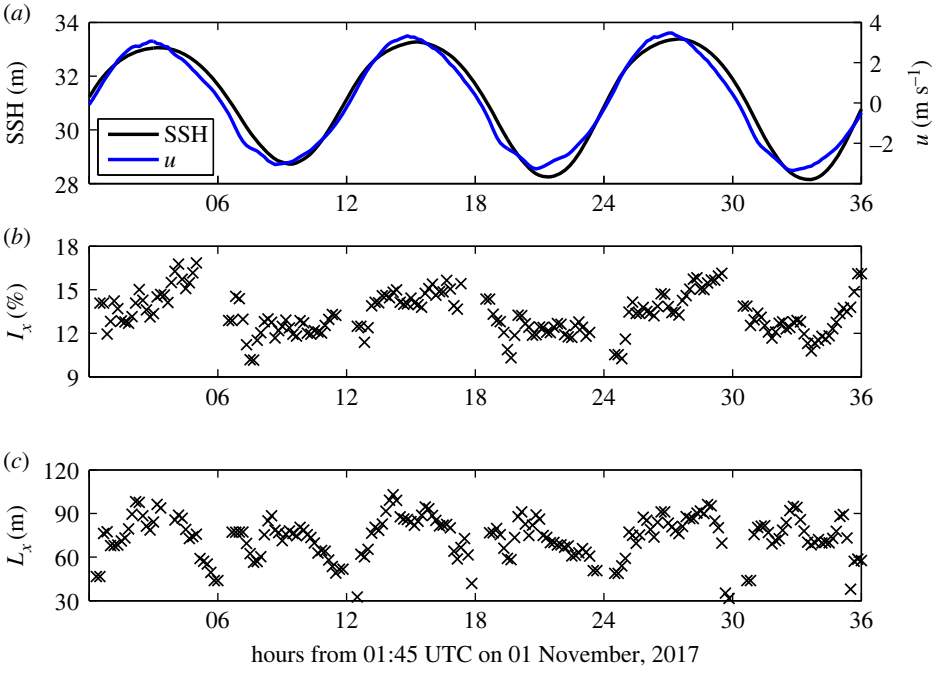

Figure 4. Time series of the SSH and velocity (*a*), turbulence intensity (*b*) and integral lengthscale (*c*), associated with the streamwise direction, at height matching the hub of the Sabella D10 ($z = 12$ m.a.b). (Online version in colour.)

is constantly higher than that associated with the spanwise and vertical direction. On average, the ratios I_x/I_y and I_x/I_z were found to be 1.2 and 3.6, respectively. The uncertainty, (ϵ_{I_i}), remains nearly constant throughout the water column with the tendency $(\epsilon_{I_y}) > (\epsilon_{I_x}) > (\epsilon_{I_z})$ (table 1). On average, the ratio ϵ_I/I, associated with the streamwise, spanwise and vertical direction was found to be 4%, 6% and 3%, respectively.

Table 1. Mean turbulence metrics and their associated uncertainty (ϵ), averaged over the 36-h long period (slack water conditions excluded) at three different heights above bottom corresponding to the lower ($z = 7$ m) and higher ($z = 17$ m) limits of the rotor blades and hub height ($z = 12$ m) of the TEC Sabella D10.

	turbulence intensity (%)			integral lengthscale (m)			Reynolds stresses ($\times 10^{-2}$ m^2 s^{-2})					
height z (m.a.b)	$I_x \pm \epsilon_{I_x}$	$I_y \pm \epsilon_{I_y}$	$I_z \pm \epsilon_{I_z}$	$L_x \pm \epsilon_{L_x}$	$L_y \pm \epsilon_{L_y}$	$L_z \pm \epsilon_{L_z}$	$\overline{u'^2} \pm \epsilon_{R_{uu}}$	$\overline{v'^2} \pm \epsilon_{R_{vv}}$	$\overline{w'^2} \pm \epsilon_{R_{ww}}$	$\overline{u'v'} \pm \epsilon_{R_{uv}}$	$\overline{u'w'} \pm \epsilon_{R_{uw}}$	$\overline{v'w'} \pm \epsilon_{R_{vw}}$
7	16.5 ± 0.5	10.5 ± 0.6	4.2 ± 0.15	62 ± 2.5	35 ± 1.0	9 ± 0.5	7.8 ± 0.7	2.8 ± 1.1	3.7 ± 0.1	1.9 ± 0.8	2.0 ± 0.15	0.4 ± 0.1
12	13.6 ± 0.5	8.6 ± 0.6	3.4 ± 0.15	74 ± 2.0	43 ± 1.5	10 ± 0.6	6.4 ± 0.6	2.2 ± 1.0	3.5 ± 0.1	2.1 ± 0.7	1.8 ± 0.1	0.35 ± 0.1
17	11.9 ± 0.5	7.7 ± 0.6	3.0 ± 0.15	84 ± 1.5	46 ± 2.0	10 ± 0.7	6.1 ± 0.6	2.3 ± 0.9	3.3 ± 0.1	1.8 ± 0.6	1.5 ± 0.1	0.3 ± 0.1

Table 2. Mean turbulence metrics estimated at our measurements site, in Alderney Race, and comparison with that obtained within other tidal channels across the world.

location	U (m s^{-1})	I_x (%)	σ_y/σ_x	σ_z/σ_x	z_n	references
Alderney Race	2.1	17.5	0.8	0.3	0.2	—
	2.5	13	0.8	0.25	0.5	
East River	2.0	12	—	—	0.5	[27]
Menai Strait	1.0	—	—	0.63	$\leq$0.2	[28]
Puget Sound	0.8–2.0	8–11	0.75	0.50	0.2	[5]
Sea Scheldt	0.8–1.4	4–5	0.90	0.63	0.9	[9]
Sound of Islay	2.0–2.5	11–13	0.70–0.75	0.50–0.55	0.1	[29]
Strangford Loch	1.5–3.5	4–9	—	—	0.5	[30]

To date, several studies focusing on the characterization of the turbulence intensity have been performed within tidal channels. Most of the studies focused on the streamwise turbulence intensity, (I_x), which is generally considered as the turbulence metric most relevant to the unsteady loading on TECs. In order to compare our results with that of others studies, the height above bottom at our site has been normalized by the mean water depth ($z = 31$ m). At similar normalized height above bottom, (z_N), the streamwise turbulence intensity quantified at our measurements site is systematically higher than that estimated at other tidal energy sites across the world (table 2). More specifically, figure 3*b* (red dashed line) shows the mean profile of the streamwise turbulence intensity (I_x), derived from ADCP measurements performed by Thomson *et al.* [5] in Puget Sound, US. Significant gaps are exhibited when comparing values of (I_x) estimated at our site with that estimated in Puget Sound. On average, the streamwise turbulence intensity calculated at a given height above bottom is almost twice as high in Alderney Race. The streamwise turbulence intensity measured in Puget Sound is even lower than the uncommonly high values of the spanwise turbulence intensity (I_y) measured at our site.

Figure 4*b* shows time series of the streamwise turbulence intensity, (I_x), calculated at height matching the hub of the Sabella D10. There, (I_x) was found to be ranging between 9% and 18% with a mean value of 13.6% (table 1). It can be seen that (I_x) is systematically lower during periods when the water level is lower than the mean level (31 m) and is higher when the water level is higher. There seems to be a quadrature between (I_x) and SSH, and therefore between (I_x) and (u). At mid-tide, (I_x) change abruptly from the highest values to the lowest one. Similar behaviour were identified for both (I_y) and (I_z) (results not shown).

(c) Integral lengthscale

The vertical variation of the integral lengthscale, (L_i), is given in figure 3*c*. The integral lengthscale associated with the streamwise and spanwise direction, i.e. (L_x) and (L_y), increases with increasing height above bottom. Both metrics were found to be ranging within the range [50 m; 90 m] and [20 m; 45 m] respectively. The integral lengthscale associated with the vertical direction, (L_z), remains nearly constant throughout the water column with a slight variation around 10 m. This result reveals that the turbulence at our measurement site is dominated by eddies, whose vertical lengthscale are about one-third of the total depth. On average, the ratios L_x/L_y and L_x/L_z were found to be 2 and 7, respectively.

The calculation of the uncertainty revealed the tendency $(\epsilon_{L_x}) > (\epsilon_{L_y}) > (\epsilon_{L_z})$ (table 1). The uncertainty (ϵ_{L_y}) and (ϵ_{L_z}) increase with increasing height above bottom whereas the opposite behaviour is exhibited for (ϵ_{L_x}). On average, the ratio ϵ_L/L associated with the streamwise, spanwise and vertical direction was found to be 3%, 3.5% and 6%, respectively. This result reveals low uncertainty, i.e. low standard error when computing the mean profile of (L_x), (L_y) and (L_z).

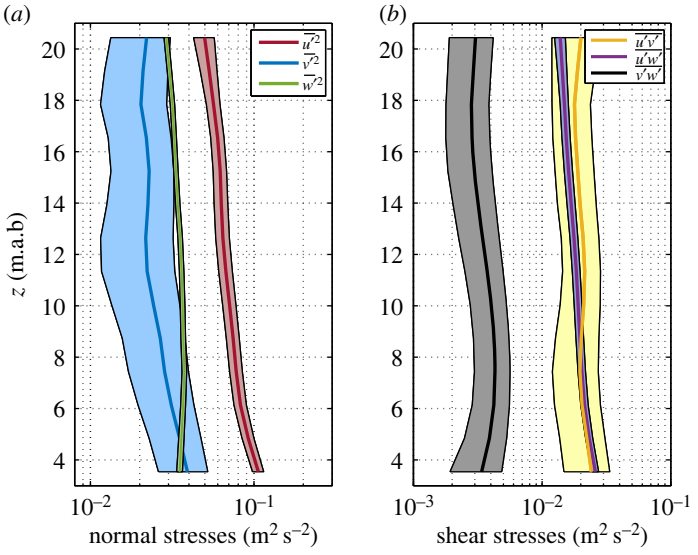

Figure 5. Mean vertical profiles (thick lines) of the normal (*a*) and shear (*b*) stresses averaged over the 36-h long period (slack water conditions excluded). Shading colours are used to identify the uncertainty, ($\epsilon_{R_{ii}}$), from the mean profile of each component of the Reynolds stress tensor. Numeric values used to build the profiles are provided alongside the present paper. (Online version in colour.)

It is clearly exhibited in figure 3*c* where the spread of shading colours (i.e. the uncertainty) is very limited. Note that the same remark is true for the turbulence intensity (figure 3*b*).

Figure 4*c* shows the time series of the integral lengthscale associated with the streamwise direction calculated at height matching the hub of the Sabella D10. There, (L_x) was found to be ranging between 30 m and 100 m with a mean of 74 m (table 1). (L_x) is clearly modulated by (u). The integral lengthscale is dependent on the flow speed and increases with increasing flow speed. Maximum integral lengthscales are associated with both peak flood and ebb velocity with values of (L_x) slightly higher during flood tide. At mid-tide, the integral lengthscale is minimum.

(d) Reynolds stresses

Figure 5 shows the mean vertical profiles of the normal and shear stresses. Both normal stresses, $\overline{u'^2}$ and $\overline{v'^2}$, as well as the shear stress $\overline{u'w'}$ decrease roughly linearly with height above bottom whereas $\overline{w'^2}$ and both shear stresses, $\overline{u'v'}$ and $\overline{v'w'}$, are almost constant throughout the water column. The component $\overline{u'^2}$ has the highest magnitude of the Reynolds stress tensor. The depth-averaged value of $\overline{u'^2}$ was found to be $7.3 \times 10^{-2}\,\mathrm{m^2\,s^{-2}}$. Both normal stresses, $\overline{v'^2}$ and $\overline{w'^2}$ are of the same order of magnitude, i.e. more or less $3.0 \times 10^{-2}\,\mathrm{m^2\,s^{-2}}$ with $\overline{w'^2}$ slightly higher than $\overline{v'^2}$. Both shear stresses, $\overline{u'v'}$ and $\overline{u'w'}$, vary little from their depth-averaged value of $2.0 \times 10^{-2}\,\mathrm{m^2 s^{-2}}$. The component $\overline{v'w'}$ has the lowest magnitude of the Reynolds stress tensor, i.e. $0.35 \times 10^{-2}\,\mathrm{m^2\,s^{-2}}$ on average. The calculation of ($\epsilon_{R_{ii}}$) shows that the maximum uncertainties are associated with the spanwise velocity (v).

The ratios of the standard deviations of the spanwise (σ_y) and vertical component (σ_z) to the streamwise velocity component (σ_x) were calculated at $z_N = 0.2$ and $z_N = 0.5$. At similar normalized height above bottom, the mean value of σ_y/σ_x was found to be of similar magnitude to that estimated at other tidal energy sites across the world (table 2). However, significant differences are exhibited when comparing the mean value of σ_z/σ_x estimated at each site. Our estimation is up to twice as low as the ratio evaluated by Heathershaw [28] in the Menai Strait.

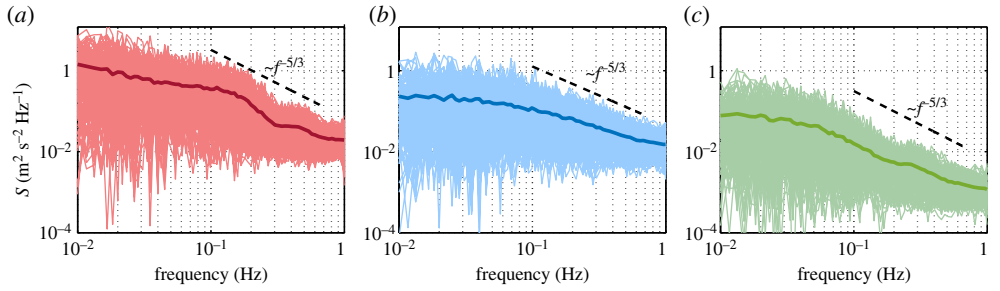

Figure 6. Individual spectra (fine curves) of the streamwise (*a*), spanwise (*b*) and vertical (*c*) velocity computed within 10-min temporal windows and at height matching the hub of the Sabella D10 ($z = 12$ m.a.b). The means of all spectra are shown as thick coloured lines. Black dashed lines show the classic spectral slope $f^{-5/3}$. Slack water conditions are excluded. (Online version in colour.)

Our lower ratio is likely due to higher streamwise turbulence intensity (I_x) and thus higher standard deviation (σ_x) measured at our site than that estimated at other sites.

(e) Velocity spectra

Figure 6 shows the spectra of the streamwise, spanwise and vertical velocity at height matching the hub of the Sabella D10. Three distinct regions are identified: the low-frequency subrange ($f \leq 0.1$ Hz), the inertial subrange ($0.1\,\text{Hz} < f < 0.7\,\text{Hz}$) and the high-frequency subrange ($f \leq 0.7$ Hz). At lower frequencies (i.e. the turbulence-production subrange), motions along the streamwise and spanwise directions are more energetic than motions along the vertical direction. This reveals a clear two-dimensional turbulence for the large-scale anisotropic eddies. At higher frequencies, spectra become flat as a result of Doppler noise. At midfrequencies, a region with a classic $f^{-5/3}$ cascade is exhibited. There, an isotropic (3D) homogeneous turbulence is expected with similar streamwise $\langle S_u \rangle$, spanwise $\langle S_v \rangle$ and vertical $\langle S_w \rangle$ energy level. Note that the brackets denote an average over the inertial subrange. However, considerable gaps in energy level were exhibited. The depth-averaged value of $\langle S_u \rangle$ was found to be 2 and 15 times higher than $\langle S_v \rangle$ and $\langle S_w \rangle$, respectively. Moreover, in this subrange, spectra associated with the streamwise velocity (figure 6*a*) were found to significantly deviate from the classic $f^{-5/3}$ slope. This pattern subsists throughout the water column (results not shown). Although the 36-h period was selected so as to avoid the turbulence measurements to be contaminated by wave-induced effects, the deviation might be a consequence of waves. Peaks in spectra derived from the streamwise velocity were observed during most strong ebb tides when the southward tidal current direction opposed the propagation of the most dominant waves.

4. Discussion

A comprehensive assessment of the turbulence-induced hydrodynamics loads on TECs is critical in order to mitigate premature failures, reduce excessive levels of conservativeness and ultimately ensure the commercial viability of TECs. In this frame, experimental turbulence measurements provide valuable information since they enable us to understand underlying dynamics of turbulent flow to ascertain the level of complexity that is required for simulating the loads and predicting fatigue life. In this paper, we present what we believe to be the first characterization of the vertical evolution of the 3D turbulence covering a large proportion of the water column at a highly energetic tidal energy site in Alderney Race.

Design studies typically assume that TECs will be aligned with current main direction in order to maximize potential yield and power take off for TECs. In this configuration, the rotor shaft and the nacelle, containing all the generating components (electrical control, generator, drive

train), will be aligned with eddies associated with the shear stress $\overline{v'w'}$. Therefore, although the magnitude of this component was found to be the lowest of the Reynolds stress tensor, we are inclined to think that $\overline{v'w'}$ will have a significant impact on the physical integrity of TECs. Moreover, the streamwise velocity was found to be associated with the component having the highest magnitude of the Reynolds stress tensor, i.e. $\overline{u'}$. This component will be responsible for high power fluctuation which is expected to deteriorate the quality of the electricity supply [31].

The dynamics of the large-scale turbulent eddies (i.e. the integral lengthscale) was found to be clearly anisotropic with predominantly horizontal motions at scales greater than the local water depth. These eddies contain the largest proportion of turbulent energy, and are therefore likely to have the greatest effect on TECs performance. Recently, a study focusing on the assessment of the performance of a Darrieus type turbine operating in real sea conditions demonstrated that the strongest impact of turbulence on power generation by the TEC occurred when the length of the most energetic eddies matches the turbine size [9]. The authors show that these eddies exert periodic loads on the blades, strongly affect torque and cause power pulsations. In view of this study, we are inclined to think that the vertical integral lengthscale, (L_z), will be responsible for significant loading on blades since (L_z) was found to match the rotor diameter of the TEC Sabella D10 (i.e. 10 m).

The large loading events are typically correlated with large-scale turbulent eddies. As the integral lengthscale is reduced, the number of large load events tends to increase, leading to high stress fatigue regime (high magnitude and moderate cycles number) [32]. Our study exhibited integral lengthscale values with the tendency $(L_x) > (L_y) > (L_z)$. In view of both this result and the conclusion of the study performed by Milne *et al.* [32], it is expected that the largest loading events will be associated with the vertical integral lengthscale, (L_z).

However, although the integral lengthscale is a dominant driver of the fatigue loads exerted on TECs blades, it is not the primary load driver for horizontal-axis TECs. A parametric assessment of the sensitivity of the fatigue loads of TEC blades indicated that the integral lengthscales have a much smaller role than the turbulence intensity [32]. In their study, the authors demonstrated that the streamwise turbulence intensity, (I_x), is the primary source of fatigue.

This metric provides a quantification of the turbulent kinetic energy contained within the flow, in a direction in which the angle of attack of the turbine blade is generally most sensitive. At a given depth, the variations of the turbulence intensity were found to be relatively low. Thus, one would expect to be able to obtain an estimate of the turbulence intensity with a good degree of confidence. Our value of (I_x) was found to be higher than that estimated at other tidal energy sites across the world for similar height above bottom. Such differences are not surprising since the turbulence intensity is a very site-specific metric influenced by factors such as bathymetry, bottom roughness or flow stratification. Considerable gaps in turbulence intensity were even exhibited at locations spaced by a few dozen metres (e.g. [33,34]). Since the bathymetry within Alderney Race is known to be very complex, it is expected that the turbulence intensity exhibits a strong spatial variation throughout the site. This highlights the need for turbine designers to gather turbulence datasets collected at the actual proposed turbine location, rather than using measurements collected at a nearby site.

Energy-spectra of the velocity were computed. It is often argued that the smallest scales of turbulence, i.e. the eddies of timescale contained within the inertial subrange, must be isotropic. However, our calculations revealed significant differences in TKE levels associated with each three-component of the velocity. Similar results were documented by Gunawan *et al.* [27]. Nonetheless, our spectra derived from time series of the along-beam velocities exhibit equivalent TKE levels within the inertial subrange, indicating a clear isotropy of the small-scale turbulence (see [13]). In view of this result, we are inclined to think that the anisotropy exhibited in the plot of the spectra associated with the streamwise, spanwise and vertical direction is an artefact of ADCP beam-spreading.

Moreover, evidence for a near $f^{-5/3}$ behaviour at the starting frequency of 0.1 Hz was shown. This frequency is consistent with that estimated at other tidal energy sites across the world

(e.g. [5,7–9,27]). Together these observations provide support for the frequency at which the inertial subrange starts being a universal property for fast-flowing natural tidal streams. The identification of the frequency at which the inertial subrange ends, however, remains strongly dependent on the type of sensors used to characterize turbulence. Typically, an ADCP does not have sufficient spatial and temporal resolution to study turbulence within the full inertial subrange. This shortcoming is due to its relatively low data output rate (2 Hz in our study) and large sampling volume. As such, an acoustic Doppler velocimeter (ADV), which has a higher data output rate (up to 64 Hz) and a smaller sampling volume than an ADCP, is often preferred for turbulence measurements.

The present analysis is based on measurements collected by conventional ADCPs. One issue with such instruments is that beams diverge with distance through the water column. This means that the area in which the measurements are being integrated increases, changing the spatial averaging of the turbulence metrics. Moreover, the determination of the 3D turbulence metrics requires a coordinate transformation across the beam of the ADCP, which assumes homogeneity. That is, the velocity vector transformation assumes that the velocities in sample bins at the same distance from the transducer are identical. This is often a reasonable assumption for mean flow velocities, which typically do not vary considerably within the spread of the acoustic beams but it is questionable when characterizing turbulence.

For the present experiment, ADCPs with a beam inclination angle of 20° were used. For example, with these instruments, the beam spread at $z = 7$ m.a.b and $z = 17$ m.a.b is 13 m and 31 m, respectively. The integral lengthscales associated with the streamwise and spanwise direction, i.e. (L_x) and (L_y), were found to be increasing with height above bottom. Because of the beam spread, the minimum value of the integral lengthscale that can be accurately resolved is increasing throughout the water column. Thus, it is likely that (L_x) and (L_y) are overestimated and that their increase with height above bottom is artificial. However, for the purpose of obtaining the turbulence intensity, the limitations of the ADCP are negligible because the larger lengthscale set the intensity [5].

A valuable alternative to ADCP is ADV. This sensor samples a small volume (approx. 1 cm cube) using usually three convergent acoustic beams to infer three components of velocity at a point. ADV takes advantage of its smaller instrument dimensions and distance to the focal point to allow both higher emitted acoustic and sampling frequencies. Nonetheless, ADVs only measure at one single point, and their deployment at a specifically chosen height requires complicated moorings and subsequent motion corrections to the raw data [35]. In addition, local measurement does not allow the identification of turbulence at all scales and deployment of multiple ADVs could affect the flow and is in any case relatively complicated.

In an effort to combine the desirable properties of both ADCP and ADV, Sellar *et al.* [36] proposed an alternative configuration of geometrically convergent acoustic beams that enable us to achieve increased spatio-temporal resolution of the velocity measurements. This configuration uses a geometrically convergent array of ADCPs. The focal point of the acoustic beams is theoretically adjustable by the attitude of the acoustic beams as well as the separation distances of the array transducers. This system allows us to reconstruct the velocity profiles with a high-resolution focal point enabling improved characterization of flow turbulence. However, challenges remain. For example, instrument ease-of-installation and robustness need to be improved [37]. The high cost of such installation is also problematic for the tidal energy industry which is struggling to generate profits.

5. Conclusion

A system of two coupled four-beam ADCPs were used to provide the vertical evolution of 3D turbulence metrics at a highly energetic site in Alderney Race. Trends are highlighted on the best way to address a dedicated methodology for structural fatigue estimation taking into account the multi-axial loadings nature of the turbulent tidal flow. Following this analysis, further works are

required to be able to define a representative 3D scatter diagram of couples (stress, frequency) with the associated occurrence in order to perform standard modal fatigue computations.

Based on these results and considering a TEC aligned with the current main direction, the main elements of turbulence prone to affect the structure (material fatigue) and to alter power generation would likely be:

— The streamwise turbulence intensity (I_x). This metric is the primary loads driver for horizontal axis-TECs. (I_x) was found to be higher at our site than that estimated at other tidal energy sites across the world.
— The shear stress, $\overline{v'w'}$. Eddies associated with $\overline{v'w'}$ will be aligned with the rotor shaft and the nacelle, which contains all the generating components, and likely the most vulnerable, of a TEC.
— The normal stress, $\overline{u'^2}$. Our results showed that the magnitude of this metric is the highest of the Reynolds stress tensor. $\overline{u'^2}$ will be responsible for high power fluctuations, thus potentially deteriorating the quality of the electricity supply.
— The vertical integral lengthscale, (L_z). The length of these large-scale eddies was found to be matching the rotor diameter of the TEC Sabella D10. These high energetic eddies are expected to cause high-stress regime of fatigue (low cycles) on the components of a TEC reducing the life expectancy of the machine.

Due to the chaotic bathymetry in Alderney Race, it is expected that these turbulence metrics vary significantly within the Race. Since an accurate fatigue design of TEC requires valuable turbulence datasets, it is strongly recommended to collect turbulence measurements at the proposed TEC location. More ideal still would be to carry out simultaneous turbulence measurements from several ADCPs spread across the planned deployment area, although the cost of this may be prohibitive.

We believe that the incorporation of intelligent turbine control schemes based on a real-time monitoring of the fatigue loads experienced by the components of the turbine would minimize the negative impact of large eddies-induced load fluctuation on both the material fatigue and the power generation.

The knowledge of the turbulence metrics generating high-frequency fatigue on the components of a TEC will enable the designers to select appropriate material components. Moreover, this will allow them to incorporate some deformation capability of the different components of their TECs in order to mitigate some of the stress distribution through key structural points.

Turbulence datasets presented in this paper represent an important support to the development of robust design tools that will improve the survivability, reliability, and performance of TECs. This new experimental data will be of interest to the tidal stream energy industry and is expected to lead to greater confidence of performance and load predictions for TECs in fast-flowing tidal streams.

Data accessibility. The data required to plot the profiles of the turbulence metrics (figures 3 and 5) are provided alongside the paper as electronic supplementary material.

Authors' contributions. M.T. drafted the manuscript and performed the 3D turbulence characterization. J.F.F., C.M., G.D., C.J., L.F.K and S.G. provided valuable comments on the manuscript and guidance on the study. S.G. was the scientific director of the THYMOTE project.

Competing interests. We declare we have no competing interest.

Funding. No funding has been received for this article.

Acknowledgements. This work benefited from funding support from France Énergies Marines and the French Government, operated by the National Research Agency under the Investments for the Future program: Reference ANR-10-IEED-0006-11. The study represents a contribution to the THYMOTE (Tidal turbulence: modelling, field observations and tank experiments) project of the above program. We also wishes to acknowledge the financial support from the Strategy for Durable Attractivity (SAD) program managed by

the Region Bretagne (Brittany). The skill and experience of Nicolas Chaplain (iXBlue) and Eloi Droniou (DynamOcean) during the fieldwork are appreciated and acknowledged.

Appendix A. Transformation matrix

The transformation matrix T is given by

$$T = \begin{pmatrix} \sin\varphi & 0 & \cos\varphi \\ -\sin\varphi & 0 & \cos\varphi \\ 0 & -\sin\varphi & \cos\varphi \\ 0 & \sin\varphi & \cos\varphi \\ 0 & 0 & 0 \\ 0 & 0 & 0 \\ 0 & 0 & 0 \\ 0 & 0 & 0 \end{pmatrix} + \begin{pmatrix} 0 & 0 & 0 \\ 0 & 0 & 0 \\ 0 & 0 & 0 \\ 0 & 0 & 0 \\ \sin\varphi & 0 & \cos\varphi \\ -\sin\varphi & 0 & \cos\varphi \\ 0 & -\sin\varphi & \cos\varphi \\ 0 & \sin\varphi & \cos\varphi \end{pmatrix}$$
$$\times \begin{pmatrix} 1 & 0 & 0 \\ 0 & \cos\phi_p & -\sin\phi_p \\ 0 & \sin\phi_p & \cos\phi_p \end{pmatrix} \begin{pmatrix} \cos\phi_r & 0 & \sin\phi_r \\ 0 & 1 & 0 \\ -\sin\phi_r & 0 & \cos\phi_r \end{pmatrix} \begin{pmatrix} \cos\phi_h & \sin\phi_h & 0 \\ -\sin\phi_h & \cos\phi_h & 0 \\ 0 & 0 & 1 \end{pmatrix}, \qquad \text{(A 1)}$$

where φ is the angle of the beams relative to the vertical. The first and second right-hand side matrices accounts for the transformation from radial velocity components to velocity in Cartesian coordinates system for the master and slave ADCP respectively. The third, fourth and fifth right-hand side matrices accounts for the rotation to match with the Cartesian coordinates system of the master ADCP. ϕ_p, ϕ_r and ϕ_h are the pitch, roll and heading, respectively, of the slave ADCP relative to the master ADCP.

References

1. Leroux T, Osbourne N, Groulx D. 2019 Numerical study into horizontal tidal turbine wake velocity deficit: quasi-steady state and transient approaches. *Ocean Eng.* **181**, 240–251. (doi:10.1016/j.oceaneng.2019.04.019)
2. Liu P, Veitch B. 2012 Design and optimization for strength and integrity of tidal turbine rotor blades. *Energy* **46**, 393–404. (doi:10.1016/j.energy.2012.08.011)
3. Milne IA, Day AH, Sharma RN, Flay RGJ. 2015 Blade loading on tidal turbines for uniform unsteady flow. *Renew. Energy* **77**, 338–350. (doi:10.1016/j.renene.2014.12.028)
4. Osalusi E, Side J, Harris R. 2009 Reynolds stress and turbulence estimates in bottom boundary layer of Fall of Warness. *Int. Commun. Heat Mass Transfer* **36**, 412–421. (doi:10.1016/j.icheatmasstransfer.2009.02.004)
5. Thomson J, Polagye B, Durgesh V, Richmond MC. 2012 Measurements of turbulence at two tidal energy sites in Puget Sound, WA, Oceanic Engineering. *IEEE J. Ocean. Eng.* **37**, 363–374. (doi:10.1109/JOE.2012.2191656)
6. Korotenko K, Sentchev A, Schmitt FG, Jouanneau N. 2013 Variability of turbulent quantities in the tidal bottom boundary layer: case study in the eastern English Channel. *Cont. Shelf Res.* **58**, 21–31. (doi:10.1016/j.csr.2013.03.001)
7. McMillan JM, Hay AE, Lueck RG, Wolk F. 2016 Rates of dissipation of turbulent kinetic energy in a high Reynolds number tidal channel. *J. Atmos. Ocean. Technol.* **33**, 817–837. (doi:10.1175/JTECH-D-15-0167.1)
8. Guerra M, Thomson J. 2017 Turbulence measurements from Five-Beam acoustic doppler current profilers. *J. Atmos. Ocean. Technol.* **34**, 1267–1284. (doi:10.1175/JTECH-D-16-0148.1)
9. Sentchev A, Thiébaut M, Schmitt FG. 2019 Impact of turbulence on power production by a free-stream tidal turbine in real sea conditions. *Renew. Energy* **147**, 1932–1940. (doi:10.1016/j.renene.2019.09.136)
10. Thiébaut M, Sentchev A, Bailly du Bois P. 2019 Merging velocity measurements and modeling to improve understanding of tidal stream resource in Alderney Race. *Energy* **178**, 460–470. (doi:10.1016/j.energy.2019.04.171)

11. Lohrmann A, Hackett B, Røed LP. 1990 High resolution measurements of turbulence, velocity and stress using a pulse-to-pulse coherent sonar. *J. Atmos. Ocean. Technol.* **7**, 19–37. (doi:10.1175/1520-0426(1990)007<0019:HRMOTV>2.0.CO;2)
12. Lu Y, Lueck RG. 1999 Using a broadband ADCP in a tidal channel. Part II: turbulence. *J. Atmos. Ocean. Technol.* **16**, 1568–1579. (doi:10.1175/1520-0426(1999)016<1568:UABAIA>2.0.CO;2)
13. Thiébaut M, Filipot J-F, Maisondieu C, Damblans G, Duarte R, Droniou E, Guillou S. 2020 Assessing the turbulent kinetic energy budget in an energetic tidal flow from measurements of coupled ADCPs. *Phil. Trans. R. Soc. A* **378**, 20190496. (doi:10.1098/rsta.2019.0496)
14. Thiébaut M, Filipot J-F, Maisondieu C, Damblans G, Duarte R, Droniou E, Chaplain N, Guillou S. 2020 A comprehensive assessment of turbulence at a tidal-stream energy site influenced by wind-generated ocean waves. *Energy* **191**, 116550. (doi:10.1016/j.energy.2019.116550)
15. Bahaj AS, Myers L. 2004 Analytical estimates of the energy yield potential from the Alderney Race (Channel Islands) using marine current energy converters. *Renew. Energy* **29**, 1931–1945. (doi:10.1016/j.renene.2004.02.013)
16. Coles DS, Blunden LS, Bahaj AS. 2017 Assessment of the energy extraction potential at tidal sites around the Channel Islands. *Energy* **124**, 171–186. (doi:10.1016/j.energy.2017.02.023)
17. Guillou N, Neill SP, Robins PE. 2018 Characterising the tidal stream power resource around France using a high-resolution harmonic database. *Renew. Energy* **123**, 706–718.
18. Vermeulen B, Hoitink AJF, Sassi MG. 2011 Coupled ADCPs can yield complete Reynolds stress tensor profiles in geophysical surface flows. *Geophys. Res. Lett.* **38**, L06406. (doi:10.1029/2011GL046684)
19. Transformation AC. 2010 Formulas and calculations. *Teledyne RD Instrum.*
20. Thiébaut M, Sentchev A. 2017 Asymmetry of tidal currents off the W. Brittany coast and assessment of tidal energy resource around the Ushant Island. *Renew. Energy* **105**, 735–747. (doi:10.1016/j.renene.2016.12.082)
21. Thomson J, Polagye B, Richmond M, Durgesh V. 2010 Quantifying turbulence for tidal power applications. In *OCEANS 2010*, pp. 1–8. IEEE.
22. McCaffrey K, Fox-Kemper B, Hamlington PE, Thomson J. 2015 Characterization of turbulence anisotropy, coherence, and intermittency at a prospective tidal energy site: observational data analysis. *Renew. Energy* **76**, 441–453. (doi:10.1016/j.renene.2014.11.063)
23. Tritton DJ. 2012 *Physical fluid dynamics*. New York, NY: Springer Science & Business Media.
24. Katul GG, Parlange MB. 1995 Analysis of land surface heat fluxes using the orthonormal wavelet approach. *Water Resour. Res.* **31**, 2743–2749. (doi:10.1029/95WR00003)
25. Kelley N, Hand M, Larwood S, McKenna E. 2002 The NREL large-scale turbine inflow and response experiment: preliminary results. In *ASME 2002 Wind Energy Symp*. American Society of Mechanical Engineers Digital Collection, pp. 412–426.
26. Kelley ND, Jonkman J, Scott N, Bialasiewicz J, Redmond L. 2005 *The Impact of Coherent Turbulence on Wind Turbine Aeroelastic Response and Its Simulation, WindPower 2005 Conf.* NREL/CP-500-38074, August.
27. Gunawan B, Neary VS, Colby J. 2014 Tidal energy site resource assessment in the East River tidal strait, near Roosevelt Island, New York, NY. *Renew. Energy* **71**, 509–517. (doi:10.1016/j.renene.2014.06.002)
28. Heathershaw AD. 1979 The turbulent structure of the bottom boundary layer in a tidal current. *Geophys. J. Int.* **58**, 395–430. (doi:10.1111/j.1365-246X.1979.tb01032.x)
29. Milne IA, Sharma RN, Flay RGJ, Bickerton S. 2013 Characteristics of the turbulence in the flow at a tidal stream power site. *Phil. Trans. R. Soc. A* **371**, 20120196. (doi:10.1098/rsta.2019.0196)
30. MacEnri J, Reed M, Thiringer T. 2013 Influence of tidal parameters on SeaGen flicker performance. *Phil. Trans. R. Soc. Lond A* **371**, 20120247. (doi:10.1098/rsta.2012.0247)
31. Lewis M, McNaughton J, Márquez-Dominguez C, Todeschini G, Togneri M, Masters I, Allmark M, Stallard T, Neill S, Goward-Brown A. 2019 Power variability of tidal-stream energy and implications for electricity supply. *Energy* **183**, 1061–1074. (doi:10.1016/j.energy.2019.06.181)
32. Milne IA, Sharma RN, Flay RGJ, Bickerton S. 2010 The role of onset turbulence on tidal turbine blade loads. In *Proc. 17th Australasian Fluid Mechanics Conf., Auckland, NZ*.
33. Gooch S, Thomson J, Polagye B, Meggitt D. 2009 *Site characterization for tidal power*. OCEANS 2009, MTS/IEEE Biloxi-Marine Technology for Our Future: Global and Local Challenges.

34. Togneri M, Masters I. 2016 Micrositing variability and mean flow scaling for marine turbulence in Ramsey Sound. *J. Ocean Eng. Mar. Energy* **2**, 35–46. (doi:10.1007/s40722-015-0036-0)
35. Thomson J, Kilcher L, Richmond M, Talbert J, DeKlerk A, Polagye B, Guerra M, Cienfuegos R. 2013 Tidal turbulence spectra from a compliant mooring. In *1st Marine Energy Technology Symp.*, Washington, D.C., April 10–11 2013, METS2013.
36. Sellar B, Harding S, Richmond M. 2015 High-resolution velocimetry in energetic tidal currents using a convergent-beam acoustic Doppler profiler. *Meas. Sci. Technol.* **26**, 085801. (doi:10.1088/0957-0233/26/8/085801)
37. Draycott S, Sellar B, Davey T, Noble DR, Venugopal V, Ingram DM. 2019 Capture and simulation of the ocean environment for offshore renewable energy. *Renew. Sustain. Energy Rev.* **104**, 15–29. (doi:10.1016/j.rser.2019.01.011)